The Journal of Neuroscience, July 1, 1999, *19*(13):5322–5331

Alternative Splicing of a Short Cassette Exon in α_{1B} Generates Functionally Distinct N-Type Calcium Channels in Central and Peripheral Neurons

Zhixin Lin, Yingxin Lin, Stephanie Schorge, Jennifer Qian Pan, Michael Beierlein, and Diane Lipscombe

Department of Neuroscience, Brown University, Providence, Rhode Island 02912

The N-type Ca channel α_{1B} subunit is localized to synapses throughout the nervous system and couples excitation to release of neurotransmitters. In a previous study, two functionally distinct variants of the α_{1B} subunit were identified, rn$\alpha_{1B\text{-}b}$ and rn$\alpha_{1B\text{-}d}$, that differ at two loci;four amino acids [SerPheMetGly (SFMG)] in IIIS3–S4 and two amino acids [GluThr (ET)] in IVS3–S4. These variants are reciprocally expressed in rat brain and sympathetic ganglia (Lin et al., 1997a). We now show that the slower activation kinetics of rn$\alpha_{1B\text{-}b}$ (ΔSFMG/+ET) compared with rn$\alpha_{1B\text{-}d}$ (+SFMG/ΔET) channels are fully accounted for by the insertion of ET in IVS3–S4 and not by the lack of SFMG in IIIS3–S4. We also show that the inactivation kinetics of these two variants are indistinguishable. Through genomic analysis we identify a six-base cassette exon that encodes the ET site and with ribonuclease protection assays demonstrate that the expression of this mini-exon is essentially restricted to α_{1B} RNAs of peripheral neurons. We also show evidence for regulated alternative splicing of a six-base exon encoding NP in the IVS3–S4 linker of the closely related α_{1A} gene and establish that residues NP can functionally substitute for ET in domain IVS3–S4 of α_{1B}. The selective expression of functionally distinct Ca channel splice variants of α_{1B} and α_{1A} subunits in different regions of the nervous system adds a new dimension of diversity to voltage-dependent Ca signaling in neurons that may be important for optimizing action potential-dependent transmitter release at different synapses.

Key words: N-type calcium channel; regulated alternative splicing; S3–S4 linker; genomic analysis; P/Q-type calcium channel; calcium channel α_1 subunits

N-type Ca channels, together with P/Q-type channels, control calcium-dependent neurotransmitter release at the majority of synapses in the mammalian nervous system (Hirning et al., 1988; Turner et al., 1992; Takahashi and Momiyama, 1993; Olivera et al., 1994; Wheeler et al., 1994; Dunlap et al., 1995). Neuronal Ca channels are also recognized as important targets for the treatment of chronic pain and neuronal degeneration after ischemic brain injury (Miljanich and Ramachandran, 1995). As the functional core of N-type Ca channels, the α_{1B} subunit contains domains critical for voltage-sensing, ion permeation (Dubel et al., 1992; Williams et al., 1992; Fujita et al., 1993), toxin binding (Ellinor et al., 1994), excitation–secretion coupling (Sheng et al., 1994), and second messenger-mediated modulation (Zamponi and Snutch, 1998). The α_{1B} subunit of the N-type Ca channel is subject to alternative splicing (Williams et al., 1992; Coppola et al., 1994; Lin et al., 1997a), but information regarding the functional significance of these splicing events is limited. We recently reported that variants of the α_{1B}-subunit that differ by four amino acids, SFMG (SerPheMetGly), in domain IIIS3–S4 and two amino acids, ET (GluThr), in domain IVS3–S4 (see Fig. 1) are differentially expressed in rat brain and sympathetic ganglia (Lin et al., 1997a). The sympathetic ganglia-dominant form of the Ca channel α_{1B}-subunit (rn$\alpha_{1B\text{-}b}$, Δ/+; see Figs. 1, 2) activates 1.5-fold slower and at potentials 7 mV more depolarized relative to the brain-dominant form (rn$\alpha_{1B\text{-}d,}$ +/Δ; see Figs. 1, 2) (Lin et al., 1997a). The relative functional impact of each of the spliced sequences (SFMG and ET) on the channel has not been determined. Furthermore, the genomic structures of these splice sites have not been characterized. It is also unclear whether alternative splicing in the functionally important S3–S4 linker region of α_{1B} is regulated similarly in all regions of the rat brain. In this study we examine these issues and also show that the functional differences between rn$\alpha_{1B\text{-}b}$ and rn$\alpha_{1B\text{-}d}$ channels may under certain conditions impact the magnitude of action potential-induced calcium transients as revealed in a model neuron. Variants of the closely related Ca channel α_{1A} subunit, which differ in the expression of two amino acids (NP) also in domain IVS3–S4, have been isolated (Yu et al., 1992; Zamponi et al., 1996; Ligon et al., 1998; Sutton et al., 1998; Hans et al., 1999). Recent studies show that these α_{1A} NP variants differ in their gating kinetics and sensitivity to block by ω-Aga IVA (Sutton et al., 1998; Hans et al., 1999), leading to the proposal that they account for P- and Q-type Ca channels described in mammalian neurons (Wheeler et al., 1994; Sutton et al., 1998). Little is known, however, about the relative abundance of α_{1A} splice variants of the NP locus in different regions of the nervous system. We begin to examine this issue by the use of the ribonuclease protection assay and establish that the NP exon in α_{1A} is also differentially expressed in different regions of the nervous system.

Preliminary reports of these findings have been presented previously in abstract form (Lin et al., 1997b; Schorge et al., 1998).

Received Jan. 13, 1999; revised April 20, 1999; accepted April 22, 1999.

This work was supported by National Institutes of Health (NIH) grants NS 29967 and NS 01927 (D.L.) and NIH Training Grant MH19118 (Z.L.). We thank Drs. Hans and colleagues for providing a copy of their manuscript before publication.

Correspondence should be addressed to Dr. Diane Lipscombe, Department of Neuroscience, Brown University, Box 1953, Providence, RI 02912.

Dr. Lin's current address: Cold Spring Harbor Laboratory, Beckman Building, 1 Bungtown Road, Cold Spring Harbor, NY 11724.

MATERIALS AND METHODS

Functional assessment of the Ca channel α_{1B} cDNA constructs

The functional properties of all Ca channel α_{1B} cDNA constructs described in this paper were assessed in the *Xenopus* oocyte expression system. All methods and procedures were essentially the same as described in Lin et al. (1997a). Robust N-type Ca channel currents were expressed in *Xenopus* oocytes after injection of α_{1B} cRNA without coexpression of exogenous Ca channel β-subunit. Heterologous expression of the Ca channel β_3 subunit along with α_{1B} increased N-type Ca channel current expression levels but did not affect channel gating kinetics nor did the presence of β_3 affect the relative differences in the time course and voltage dependence of activation of the α_{1B} splice variants (Lin et al., 1997a). *Xenopus* oocytes do express, however, an endogenous Ca channel β-subunit (β_{3XO}) (Tareilus et al., 1997) that is highly homologous to the mammalian β_3. It is possible that the *Xenopus* β_{3XO} associates with and modulates heterologously expressed α_{1B} in the oocyte. This may explain why coexpression of heterologous β_3 is not required for functional expression of N-type Ca channels in this system (Tareilus et al., 1997). cRNAs were *in vitro* transcribed using the mMESSAGE mMACHINE kit (Ambion) from the various α_{1B} cDNA constructs subcloned into the *Xenopus* β-globin expression vector (pBSTA) (Goldin and Sumikawa et al., 1992). A cRNA solution (46 nl of 750 ng/μl) was injected into defolliculated oocytes using a precision nanoinjector (Drummond). N-type Ca channel currents were recorded 6–7 d after injection. At least 15 min before recording, oocytes were injected with 46 nl of a 50 mM solution of 1,2-bis(*o*-aminophenoxy)ethane-*N,N,N′,N′*-tetraacetate (BAPTA). This we have found critical to minimize activation of an endogenous Ca-activated Cl^- current, even when Ba^{2+} is the charge carrier (Lin et al., 1997a). Cells exhibiting slowly deactivating tail currents, indicative of the presence of Ba^{2+}-dependent activation of the Ca-activated Cl^- current, were excluded from the analyses.

N-type Ca channel currents were recorded from oocytes using the two-microelectrode voltage-clamp recording technique (Warner amplifier; OC-725b). Micropipettes of 0.8–1.5 and 0.3–0.5 MΩ resistance when filled with 3 M KCl were used for the voltage and current recording electrodes, respectively. Oocytes expressing Ca channel currents usually had resting membrane potentials between −40 and −50 mV when impaled with two electrodes. A grounded metal shield was placed between the two electrodes to increase the settling time of the clamp. Recording solutions contained 5 mM $BaCl_2$, 85 mM tetraethylammonium, 5 mM KCl, and 5 mM HEPES, pH adjusted to 7.4 with methanesulfonic acid. The recording temperature was between 19° and 22°C.

The properties of each mutant construct were assessed by expressing it together with appropriate controls (ΔET α_{1B} and +ET α_{1B}). Each mutant was tested in three separate batches of oocytes, and within each batch recordings were made from at least six oocytes for each mutant construct and control. Recordings from the oocytes expressing the various Ca channel α_{1B} constructs were randomized throughout the data collection period.

Data analysis. Data were acquired on-line and leak-subtracted using a P/4 protocol (PClamp V6.0; Axon Instruments). Voltage steps were applied every 10–30 sec depending on the duration of the step, from a holding potential of −80 mV. Ca channel currents recorded under these conditions showed little run-down over the duration of the recordings. Three sets of current–voltage relationships were obtained from each cell using step depolarizations of 26.3 msec, 650 msec, and 2.6 sec in duration and digitized at 25 kHz, 10 kHz, and 250 Hz, respectively. Exponential curves (activation and inactivation) were fit to the data using curve-fitting routines in PClamp (Axon Instruments) and Origin (Microcal). Inactivation time constants in the range of 70–800 msec were estimated from currents evoked by the longest depolarizations (2.6 sec). Activation time constants were best resolved from currents evoked by the shortest depolarizations (26.3 msec; sampled at 25 kHz).

Ribonuclease protection assay

The procedures are essentially the same as those described in Lin et al. (1997a). Total RNA was purified from various neuronal tissues of adult rats using a guanidium thiocyanate and phenol-chloroform extraction protocol [adapted from Chomczynski and Sacchi (1987)]. ^{32}P-labeled antisense RNA probes overlapping ET [nucleotide (nt) 4379–4836] in rn$\alpha_{1B\text{-}b}$ and NP (nt 4605–4930) in rbα_{1A} (Starr et al., 1991) were constructed from linearized plasmids (pGEM-T vector) containing appropriate RT-PCR-derived subclones using the Maxi-script kit (Ambion). Probes were gel-purified and stored as ethanol precipitates. RNA (1 μg) purified from sympathetic or sensory ganglia or RNA (5 μg) isolated from various CNS tissues was precipitated with 2×10^5 cpm of probe and resuspended in 30 μl hybridization buffer containing 60% formamide, 0.4 M NaCl, 10 mM EDTA, and 40 mM PIPES at pH 6.4. Samples were denatured at 85°C and allowed to hybridize overnight at 60°C. The samples were then digested in a 350 μl reaction mix containing 0.3 M NaCl, 5 mM EDTA, 3.5 μl of the RNase mixture (Ambion), and 10 mM Tris at pH 7.5, then treated with proteinase K, extracted, and precipitated with 10 μg of tRNA as carrier. After resuspension in 30 μl formamide loading buffer, the samples were denatured and separated on a 5% polyacrylamide gel. After exposure to a phosphorimaging plate to quantify relative band intensities (Fuji BAS 1000), the gel was subsequently exposed to film with an intensifying screen for 4–5 d at −80°C.

Site-directed mutagenesis

A recombinant PCR-based technique was used to introduce mutations (QT, EA, AT, AA, NP) at the ET site in the IVS3–S4 linker of $\alpha_{1B\text{-}b}$. A pair of primers 5′-attcttgtggtcatcgccttgag (Bup 3460) and 5′-gacaggcctccaggagcttggtg (Bdw 5623) flanked a region of the clone that contained two restriction sites, RsrII (nt 3510) and *Bgl*II (nt 5465), located either side of ET (nt 4674). A second primer pair contained the desired mutation and directly overlapped the ET site (Bdwmut and Bupmut; see below). Two separate PCRs were performed with Bup 3460 and Bdwmut, and Bupmut and Bdw 5623. The PCR product then served as template for a second round of PCR using Bup 3460 and Bdw 5623, generating the final mutant PCR fragment that was subsequently subcloned into rn$\alpha_{1B\text{-}b}$ at the Rsr II and *Bgl*II sites. Mutants were screened by restriction digest and confirmed by DNA sequencing. All PCR was performed using Expand High Fidelity (Boehringer Mannheim, Indianapolis, IN). The mutagenesis primers used were as follows: ET/AT: Bupmut 5′-gagattgcg**GCAACG**aacaacttcatc-3′; Bdwmut 5′-aagttgtt**CGTTTC**cgcaatctccg-3′; ET/QT: Bupmut 5′-gagattgcg**CAGACG**aacaacttcatc-3′; Bdwmut 5′-aagttgtt**CGTCTG**cgcaatctccg-3′; ET/EA: Bupmut 5′-gagattgcg**GAAGCT**aacaacttcatc-3′; Bdwmut 5′-aagttgtt**AGCTTC**cgcaatctccg-3′; ET/AA: Bupmut 5′-gagattgcg**GCAGCT**aacaacttcatc-3′; Bdwmut 5′-aagttgtt**AGCTGC**cgcaatctccg-3′; ET/NP: Bupmut 5′-gagattgcg**AACCCT**aacaacttcatc-3′; Bdwmut 5′-aagttgtt**AGGGTT**cgcaatctccg-3′.

Genomic analysis

The IVS3–S4 region of the rat α_{1B} and α_{1A} genes were analyzed by genomic PCR. Primer pairs were directed to the IVS3 and IVS4 membrane-spanning regions that were presumed to reside in the 5′ and 3′ exons flanking the ET and NP insertions of the α_{1B} and α_{1A} genes, respectively. PCR was performed in a 50 μl reactions mix containing 250 ng rat liver genomic DNA, 250 μM each nucleotide, and 0.4 μM each primer. After a preincubation for 15 min at 92°C, 0.75 μl enzyme mix was added to start the amplification. The resultant gDNA products were gel-purified, cloned into pGEM-T (Promega), and sequenced. The α_{1B} primers generated two bands of ~11 kb and ~900 bases. The 11 kb band was derived from the α_{1B} gene and contained the desired ET encoding exon in IVS3–S4. The 900 base product resulted from amplification of the equivalent site in the α_{1E} gene that contained a relatively short ~700 bp intron and no intervening exon. The α_{1A} primers generated a single 9 kb PCR product that was confirmed to be derived from the α_{1A} gene by DNA sequencing (Yale University sequencing facility). Primers were as follows: α_{1A}: Aup4737 5′-tgcctggaacatcttcgactttgtga; Adw4876 5′-cagaggagaatgcggatggtgtaacc; and α_{1B}: Bup4599 5′-cagagatgcctggaacgtctttgac; Bdw4744 5′-ataacaagatgcggatggtgtagcc.

Modeling Ca entry

A one-compartment cell model using standard compartmental modeling techniques in NEURON (Hines and Carnevale, 1997) was used to predict the amount of Ca entering a neuron expressing either rn$\alpha_{1B\text{-}b}$ or rn$\alpha_{1B\text{-}d}$ N-type Ca channel currents. The cell had a total membrane area of 1250 μm^2, 0.75 $\mu F/cm^2$ specific membrane capacitance, and 30 $k\Omega cm^2$ specific membrane resistance. For action potential simulation a fast sodium conductance (g_{Na}) and a delayed rectifying potassium conductance ($g_{K,DR}$) were included (Mainen and Sejnowski, 1995), each with densities of 300 pS/μm^2. Ca^{2+} influx was mediated by a fast calcium conductance (g_{Ca}) (Yamada et al., 1989) with a density of 1 pS/μm^2. Action potentials were evoked by a 5 msec, 400 pA current step. Resultant currents were calculated using conventional Hodgkin-Huxley kinetic schemes according to the formulae given below. The resting membrane potential was set at −70 mV, and Na and K current reversal potentials

were set at +50 mV and −75 mV, respectively. The calcium current was computed using the Goldman-Hodgkin-Katz equation. Extracellular Ca concentration was 2.5 mM, and the intracellular Ca concentration was computed using entry via I_{Ca} and removal via a first order pump $d[Ca^{2+}]_i/dt = (-1 \cdot 10^5 \cdot I_{Ca}/2F) - ([Ca^{2+}]_i - [Ca^{2+}]_\infty)/\tau_R$, where $[Ca^{2+}]_\infty = 100$ nM and $\tau_R = 80$ msec. The simulation does not incorporate mobile or immobile Ca buffers. The time constants and maximal Ca channel conductances used in this model were measured at room temperature. These values were adjusted for simulation at 37°C based on Q_{10} values of 1.5 and 3.0 for the conductance and activation kinetics, respectively (Cota et al., 1983). Formulae used for calculation of various currents were as follows: sodium current (I_{Na}), $m^3 \cdot h$: $\alpha_{m,\,Na} = 0.182 \cdot (v + 25)/(1 - e^{-(v+25)/9})$; $\beta_{m,\,Na} = -0.124 \cdot (v + 25)/(1 - e^{(v+25)/9})$; $\alpha_{h,\,Na} = 0.024 \cdot (v + 40)/(1 - e^{-(v+40)/5})$; $\beta_{h,\,Na} = -0.0091 \cdot (v + 65)/(1 - e^{(v+65)/5})$; $h_{\infty,\,Na} = 1/(1 + e^{(v+55)/6.2})$; delayed recifier ($I_{K(DR)}$), m: $\alpha_{m,\,K(DR)} = 0.02 \cdot (v - 25)/(1 - e^{-(v+25)/9})$; $\beta_{m,\,K(DR)} = -0.002 \cdot (v - 25)/(1 - e^{(v+25)/9})$; high threshold, N-type rn$\alpha_{1B\text{-}b}$ calcium current (I_{ca}), $m \cdot h$: $m_{\infty,\,Ca} = 1/(1 + e^{-(v-3)/8})$; $\tau_{m,\,Ca} = 7.8/(e^{(v+6)/16} + e^{-(v+6)/16})$; $h_{Ca} = K/(K + [Ca^{2+}]_i)$ with K = 0.01 mM. The brain-dominant form, rn$\alpha_{1B\text{-}d}$, was modeled by shifting the voltage dependence of the N-type Ca channel conductance activation variable ($m_{\infty,\,Ca}$) by −7 mV and decreasing the activation time constant by 1.5-fold (Lin et al., 1997a) (see Fig. 2*A*).

RESULTS

Alternative splicing in the putative S3–S4 extracellular linkers affects channel activation but not inactivation kinetics

In a previous study we showed that rn$\alpha_{1B\text{-}b}$ (ΔSFMG/+ET) and rn$\alpha_{1B\text{-}d}$ (+SFMG/ΔET) N-type currents differ with respect to their gating kinetics when expressed in *Xenopus* oocytes [compare Δ/+ and +/Δ in Fig. 2*A,B*; see also Lin et al. (1997a)]. We reported apparent differences in both the macroscopic rates of channel activation and the inactivation between the two splice variants, but because relatively short duration depolarizations were used, the inactivation kinetics were not fully resolved. Consequently, and as discussed in Lin et al. (1997a), it was difficult to ascribe the differences in gating kinetics between the N-type Ca channel α_{1B} splice variants exclusively to differences in either channel activation or inactivation mechanisms. In the present study we have used both short (26 msec) and long (2.6 sec) depolarizations to resolve the time course of Ca channel activation *and* inactivation. rn$\alpha_{1B\text{-}b}$ (Δ/+) (Fig. 1) and rn$\alpha_{1B\text{-}d}$ (+/Δ) (Fig. 1) subunits were expressed in *Xenopus* oocytes, and the resulting N-type Ca channel currents were recorded using 5 mM Ba as the charge carrier (Figs. 2, 3). N-type Ca channel currents evoked by depolarizations to 0 mV or higher inactivated with a bi-exponential time course (τ_{fast} 100–150 msec and τ_{slow} 700–800 msec) (Fig. 3*A*). The inactivation time constants of the cloned channels expressed in *Xenopus* oocytes (rn$\alpha_{1B\text{-}b}$, Δ/+ and rn$\alpha_{1B\text{-}d}$, +/Δ) (Fig. 3*A,B*) were weakly voltage dependent, consistent with studies of native N-type Ca channels of bullfrog sympathetic neurons (Jones and Marks, 1989). Figure 3*A,B* shows that the fast and slow inactivation time constants of rn$\alpha_{1B\text{-}b}$ and rn$\alpha_{1B\text{-}d}$ currents evoked by relatively long duration step depolarizations to between 0 mV and +30 mV were not significantly different. In contrast, the rates of channel activation of the two variants in the same cells were significantly different (Fig. 2*A,B*). On the basis of these observations we conclude that alternative splicing in domains IIIS3–S4 and IVS3–S4 of the α_{1B} subunit alters the time course of N-type Ca channel activation but has no direct effect on inactivation kinetics. The apparent differences in the time courses of inactivation previously reported for rn$\alpha_{1B\text{-}b}$ and rn$\alpha_{1B\text{-}d}$ using relatively short duration depolarizing pulses (Lin et al., 1997a) can thus be ascribed to differences in their rates of channel activation, not inactivation. A selective effect on channel activation kinetics is consistent with the close proximity of the spliced sites, S3–S4 linkers, to their respective S4 helices that are the putative voltage sensors of the six transmembrane family of voltage-gated ion channels (Hille, 1992). In contrast, the domains of the Ca channel α_{1B} subunit implicated in voltage-dependent inactivation of N-type Ca channels (IS6 and flanking putative extracellular and intracellular linkers) (Zhang et al., 1994) are likely to be more distant from the S3–S4 linker splice sites.

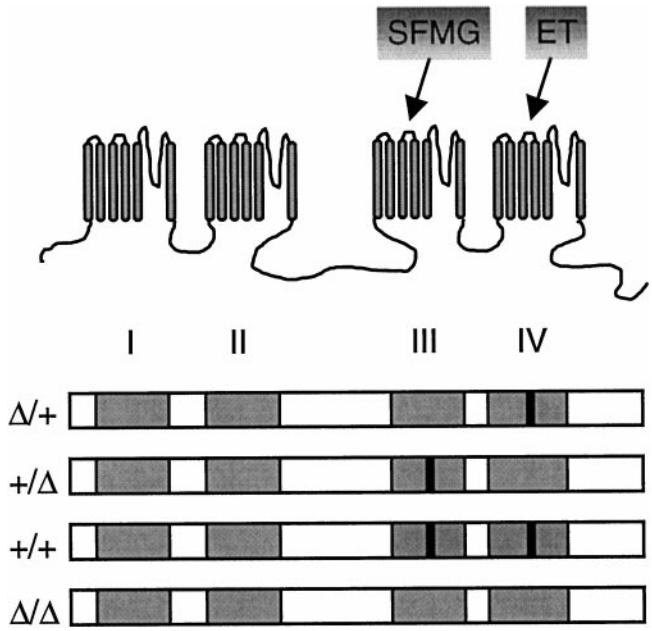

Figure 1. The location of two alternatively spliced sequences in the S3–S4 extracellular linkers of domains III and IV of the Ca channel α_{1B} subunit. *Top*, Putative membrane topology of the Ca channel α_{1B} subunit and location of two alternatively spliced sequences encoding SerPheMetGly (*SFMG*) and GluThr (*ET*) in the S3–S4 linkers of domains III and IV. *Bottom*, Four α_{1B} clones differing in the presence of SFMG and ET encoding sequences (Δ/+, +/Δ, +/+, Δ/Δ) used to evaluate their relative effects on channel gating kinetics (Fig. 2).

Splicing of ET in domain IVS3–S4 underlies the major functional difference between rn$\alpha_{1B\text{-}b}$ and rn$\alpha_{1B\text{-}d}$

rn$\alpha_{1B\text{-}b}$ and rn$\alpha_{1B\text{-}d}$ differ in composition by six amino acids located in two distinct regions of the Ca channel α_{1B} subunit (SFMG in domain IIIS3–S4 and ET in domain IVS3–S4) (Fig. 1). To separate the relative contribution of SFMG in domain IIIS3–S4 and ET in domain IVS3–S4 to the different gating kinetics observed between rn$\alpha_{1B\text{-}b}$ (ΔSFMG/+ET) and rn$\alpha_{1B\text{-}d}$ (+SFMG/ΔET) we constructed two additional clones, +/+ and Δ/Δ (Fig. 1) and compared the functional properties of all four clones. Figure 2*A,B* demonstrates that the presence of the dipeptide sequence ET in domain IVS3–S4 is directly correlated with the altered activation kinetics of rn$\alpha_{1B\text{-}b}$ currents compared with rn$\alpha_{1B\text{-}d}$. Activation time constants measured from N-type Ca channel currents in oocytes expressing clones Δ/+ (rn$\alpha_{1B\text{-}b}$) and +/+ were indistinguishable and 1.5-fold slower on average than those induced by the expression of clones +/Δ (rn$\alpha_{1B\text{-}d}$) and Δ/Δ (Fig. 2*A,B*). The presence of ET in domain IVS3–S4 also influenced the voltage-dependence of channel activation. A comparison of the midpoints of the rising phase of the peak current–voltage plots ($V_{1/2}$) generated for the two ET containing clones Δ/+ (rn$\alpha_{1B\text{-}b}$; −7.8 ± 0.6 mV, $n = 6$) and +/+ (−9.7 ± 1.0 mV,

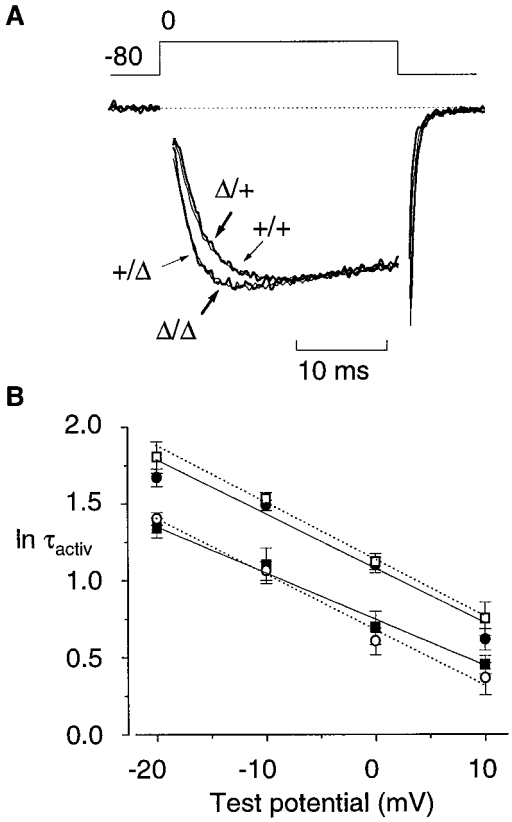

Figure 2. The presence of ET in domain IVS3–S4 of α_{1B} slows the rate of N-type Ca channel activation. *A, B*, Ca channel α_{1B} subunits that differ in the expression of ET in the IVS3–S4 linker activate at different rates. *A*, Averaged, normalized Ca channel current induced by the expression in *Xenopus* oocytes of four different α_{1B} constructs (see Fig. 1). Currents were evoked by step depolarizations to 0 mV from a holding potential of −80 mV. Each trace represents the average, normalized current calculated from at least six oocytes. SFMG-containing clones are distinguished from SFMG-lacking clones by *thin* and *thick lines*, respectively. *B*, Plot of average activation time constants (ln τ_{activ}) at different test potentials (between −20 and +10 mV) for clones +/+ (□), Δ/+ (●), +/Δ (○), and Δ/Δ (■). The presence of SFMG in domain IIIS3–S4 did not affect the rate of channel activation. There was no significant difference in τ_{activ} between clones +/+ and Δ/+ or between clones +/Δ and Δ/Δ ($p > 0.1$ at all test potentials between −20 mV and +10 mV). The presence of ET in domain IVS3–S4 slowed channel activation kinetics. τ_{activ} values for clones +/+ and Δ/+ were significantly slower compared with +/Δ and Δ/Δ, at all test potentials between −20 mV and +10 mV ($p < 0.05$).

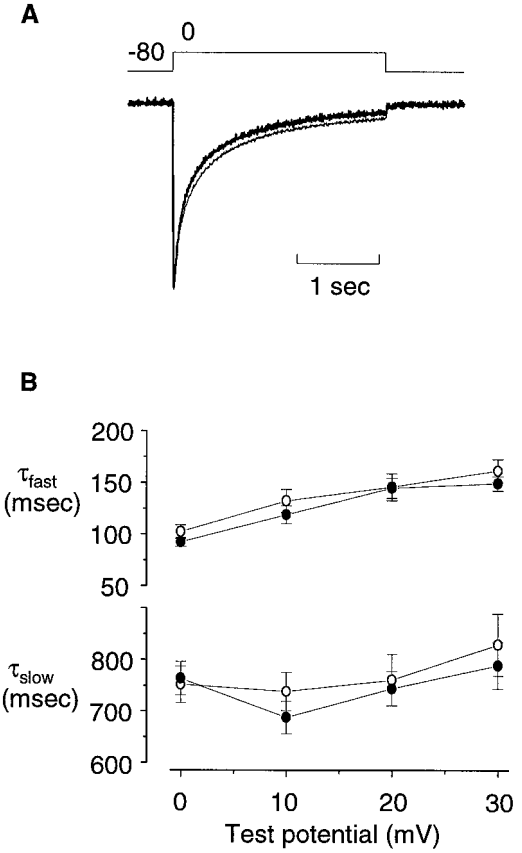

Figure 3. Alternative splicing in the S3–S4 linkers of domains III and IV of α_{1B} does not affect channel inactivation kinetics. *A, B*, The rate of N-type Ca channel inactivation is not affected by the presence of SFMG or ET in the S3–S4 linkers of domains III and IV. *A*, Ca channel currents recorded from oocytes expressing rn$\alpha_{1B\text{-}b}$ (ΔSFMG/+ET, *thick line*) and rn$\alpha_{1B\text{-}d}$ (+SFMG/ΔET, *thin line*). Currents were evoked by 2.6 sec depolarizations to 0 mV from a holding potential of −80 mV. Each trace represents the average, normalized current calculated from at least six oocytes. *B*, Plot of the fast and slow inactivation time constants of currents at different test potentials. There is no significant difference between the fast and slow inactivation time constants calculated for rn$\alpha_{1B\text{-}b}$ (●) and rn$\alpha_{1B\text{-}d}$ (○) at test potentials between 0 mV and +30 mV ($p > 0.1$). Each point is the average value ± SE ($n > 5$).

$n = 6$) shows that they are not significantly different from each other ($p > 0.05$, Student's t test). Likewise, $V_{1/2}$ values estimated from two ET-lacking constructs, +/Δ (rn$\alpha_{1B\text{-}d}$; −15.4 ± 0.4 mV, $n = 7$) and Δ/Δ (−13.4 ± 0.7, $n = 6$), were not significantly different from each other ($p > 0.05$) and activated at potentials that were, on average, 6 mV more negative compared with ET-containing clones Δ/+ and +/+ (data not shown). Although the presence of ET in domain IVS3–S4 dominates in regulating the voltage dependence of activation, the analysis does reveal a small contribution of SFMG. SFMG-containing clones (+/Δ and +/+) activated at potentials that were 2 mV hyperpolarized compared with those that lacked SFMG (Δ/+ and Δ/Δ). A 2 mV shift in the voltage dependence of activation was not significant at the 5% level, in a comparison of $V_{1/2}$ values from clones Δ/+ and +/+, but did reach significance in a comparison of +/Δ and Δ/Δ ($p < 0.025$, Student's t test).

The pattern of expression of ET-containing Ca channel α_{1B} mRNA in different regions of the nervous system

Figure 2 indicates that alternative splicing of ET within domain IVS3–S4 of the Ca channel α_{1B} subunit accounts for the major functional differences between rn$\alpha_{1B\text{-}b}$ and rn$\alpha_{1B\text{-}d}$. This prompted us to systematically analyze the expression pattern of the six bases in α_{1B} mRNA that encoded ET. We had shown previously that ET-containing α_{1B} (+ET α_{1B}) mRNA was in very low abundance in total rat brain extracts (Lin et al., 1997a). To determine whether ET-lacking α_{1B} (ΔET α_{1B}) mRNA dominated throughout the CNS we used the ribonuclease protection assay and analyzed RNA isolated from spinal cord, cerebellum, cortex, hippocampus, hypothalamus, medulla, and thalamus of adult rats (Fig. 4). In all regions tested >90% of the α_{1B} mRNA expressed in the CNS lacked the ET encoding sequence. In contrast, in sympathetic and sensory ganglia the majority of α_{1B} mRNA contained the ET encoding sequence (Fig. 4). Together these findings suggest that +ET α_{1B} subunits are primarily restricted to neurons of the peripheral nervous system. Consistent with this we have analyzed RNA isolated from human brain and trigeminal

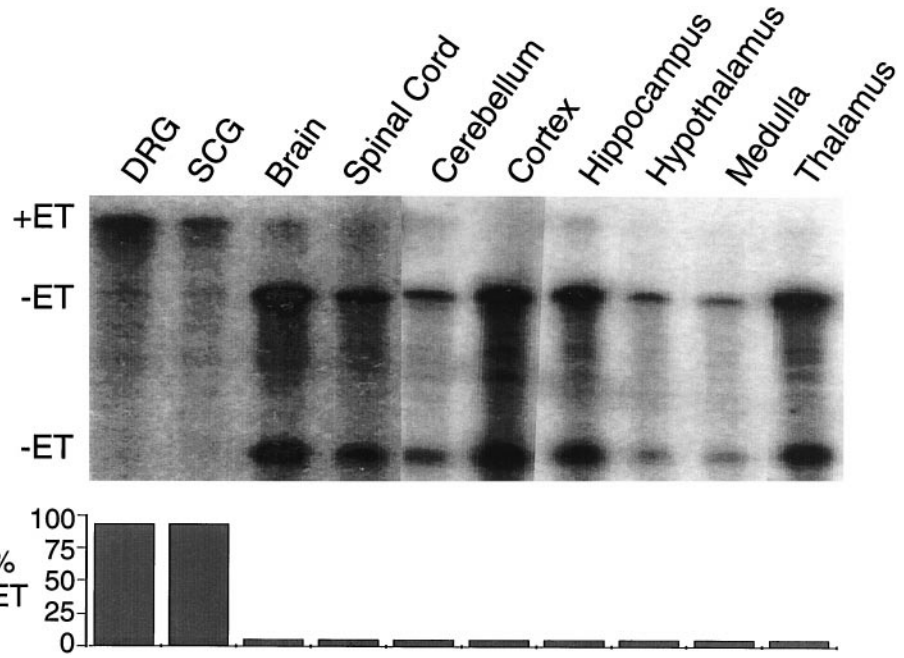

Figure 4. The expression pattern of ETα_{1B} splice variants in various regions of the rat nervous system. RNase protection analysis of α_{1B} RNA isolated from dorsal root ganglia (*DRG*), superior cervical ganglia (*SCG*), and various brain regions of adult rats using a complimentary probe that extends from nt 4379 to nt 4836 and contains the ET insert at nt 4675. *Top*, Gel separation of RNase digested ^{32}P-labeled probe hybridized to the various RNA samples. The strong signal corresponding to fully protected probe (*+ET*, 463 bases) in the DRG and SCG lanes indicates a predominance of +ETα_{1B} RNA. The two shorter bands (*−ET*, 296 and 161 bases) most prominent in the CNS lanes correspond to cleaved probe, indicating high levels of ET-lacking α_{1B} RNA. *Bottom*, Average levels of +ETα_{1B} RNA calculated from at least three separate experiments. In all regions of the brain tested, >90% of the α_{1B} RNA lacked the ET encoding sequence, whereas in ganglia ~80% α_{1B} RNA contained the ET sequence. RNA products were separated on a 5% acrylamide gel, and relative band intensities were calculated using a phosphorimager.

ganglia and observed analogous patterns of expression: low levels of +ETα_{1B} mRNA in brain (~10%) and high levels (~70%) in ganglia (S. Schorge and D. Lipscombe, unpublished data).

Site-directed mutagenesis within IVS3–S4

Having shown that alternative splicing of the ET encoding sequence in the IVS3–S4 linker of α_{1B} has a significant effect on the kinetics and voltage dependence of N-type Ca channel gating, we next used site-directed mutagenesis to determine the relative importance of each amino acid, glutamate and threonine. A series of mutants in which ET was replaced with either QT, AT, EA, AA, or NP were constructed (Fig. 5) from clone Δ/+ (rn$\alpha_{1B\text{-}b}$), which served as the background structure. The mutant constructs were then expressed in *Xenopus* oocytes, and their properties were compared with clones +ET (100% slow; Fig. 5) and ΔET (100% fast; Fig. 5). All mutants expressed equally well in the *Xenopus* oocyte expression system.

The role of the glutamate in domain IVS3–S4 was of major interest because it should be negatively charged at neutral pH and consequently might influence the gating machinery of the channel via electrostatic interactions. Figure 5, however, shows that replacing glutamate with glutamine resulted in a channel that activated only slightly faster than +ET α_{1B} (Fig. 5, *QT*). Substituting alanine for glutamate (AT) decreased τ_{act}, but consistent with the QT mutant, suggests that the presence of a negative charge in IVS3–S4 (glu) does not underlie the slow gating kinetics of the +ETα_{1B} variant. Similarly, alanine substitution of either threonine alone (EA) or together with glutamate (AA) generated channels with activation kinetics that were intermediate between +ET α_{1B} and ΔET α_{1B} clones. Together, these results suggest that the presence of both glutamate and threonine in the IVS3–S4 linker is necessary to reconstitute the relatively slow channel opening rates characteristic of N-type Ca channel α_{1B}-subunits that dominate in sensory and sympathetic ganglia.

Evidence for alternative splicing in the IVS3–S4 linker regions of the α_{1B} and α_{1A} genes

The existence of an alternatively spliced exon in the IVS3–S4 region of the rat Ca channel α_{1B} gene has been hypothesized (Lin et al., 1997a) but not yet confirmed. Genomic analysis was therefore undertaken to locate the splice junctions in the IVS3–S4 region of the α_{1B} gene and to pinpoint the precise location of the putative six-base, ET-encoding exon. PCR amplification from rat genomic DNA using primers designed to hybridize to the transmembrane spanning S3 and S4 helices flanking IVS3–S4 in α_{1B} revealed the presence of a long ~10 kb stretch of intron sequence. DNA sequencing established the location of exon/intron and intron/exon boundaries and conserved ag–gt splice junction signature sequences immediately 5′ and 3′ to the putative ET insertion site (Fig. 6*A*, α_{1B}). A six-base cassette exon encoding ET was located 8 kb into the 5′ intron and establishes that ET-α_{1B} variants are generated by alternative splicing. Sequence comparisons of several cDNAs encoding α_1 subunits of other voltage-gated Ca channels suggests that alternative splicing in the IVS3–S4 linker could be a general mechanism for regulating voltage-dependent Ca channel gating (Fig. 6*B*). This has recently been demonstrated for α_{1A} (Sutton et al., 1998; Hans et al., 1999), a Ca channel subunit that is closely related both structurally and functionally to the N-type Ca channel α_{1B}-subunit. A comparison of the IVS3–S4 region of various mammalian α_{1A} cDNAs derived from kidney, pancreas, and brain (Fig. 6*B*) (Yu et al., 1992; Ligon et al., 1998; Sutton et al., 1998; Hans et al., 1999) is consistent with alternative splicing of six bases encoding asp, pro (NP) in this region. The exon/intron structure in the IVS3–S4 linker region of the closely related rat α_{1A} gene was therefore also determined (Fig. 6*A*). The rat α_{1A} gene contained a long stretch of intron sequence (~8 kb) and ag–gt splice junctions at the 5′ (gt) and 3′ (at) ends of the intronic segment (Fig. 6*A*). We have not yet determined the precise location of the NP encoding cassette exon in the rat α_{1A} gene but conclude that it must reside within the 8 kb of intron sequence in the IVS3–S4 linker region. Tissue-specific alternative splicing of six-base cassette exons in the IVS3–S4 linkers of both α_{1A} and α_{1B} explains the presence of splice variants of these subunits in the mammalian brain and underscores the high level of conservation between these two functionally related genes. We have also analyzed the genomic structure of the more distantly related rat α_{1E} gene that encodes

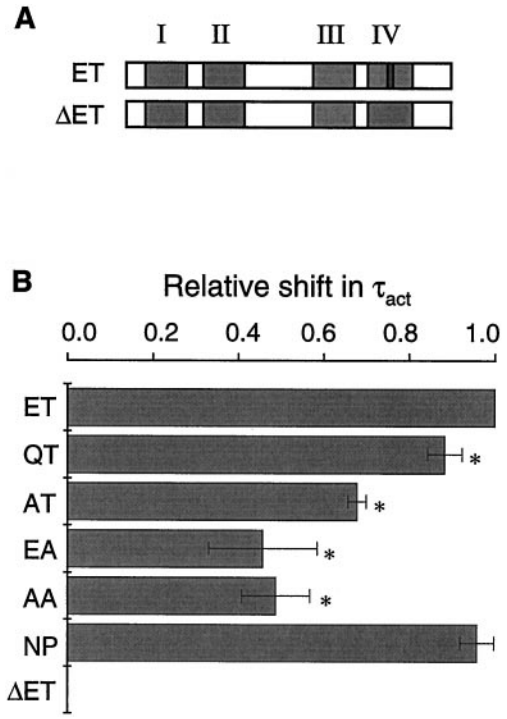

Figure 5. Functional analysis of site-directed mutagenesis of the ET splice site in domain IVS3–S4 of the α_{1B} subunit. Activation time constants were estimated from currents induced by the expression of the various mutant α_{1B} constructs (*QT, AT, EA, AA, NP*) in oocytes and compared with clones ET and ΔET (*A*). Shifts in the activation time constants of the mutant channels, relative to clones ET (100% slow) and ΔET (100% fast) are plotted (*B*). Each point represents data collected from at least 18 oocytes per mutant (each mutant was tested in three separate batches of oocytes, and within each experiment at least six oocytes per mutant were analyzed). Values plotted are means ± SEs from the three data sets. The *asterisk* indicates a significant slowing of the activation time constant compared with clone ET ($p < 0.05$).

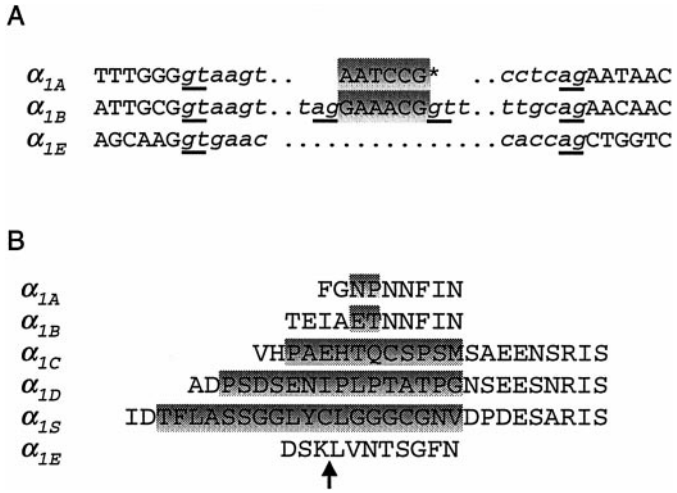

Figure 6. Alternative splicing in the IVS3–S4 linker region of different Ca channel α_1 genes. *A*, An alignment of amino acid sequences IVS3–S4 linkers of six different Ca channel α_1 subunits derived from rat tissue. *Shaded regions* indicate probable sites of alternative splicing based on the identification of α_1 cDNAs variants in the IVS3–S4 region for all but the α_{1E} subunit (α_{1A}: Starr et al., 1991; Yu et al., 1992; Zamponi et al., 1996; Ligon et al., 1998; Sutton et al., 1998; Hans et al., 1999; α_{1B}: Dubel et al., 1992; Williams et al., 1992; Lin et al., 1997a; α_{1C}: Perez-Reyes et al., 1990; Snutch et al., 1991; Barry et al., 1995; α_{1D}: Barry et al., 1995; Ihara et al., 1995; α_{1E}: Soong et al., 1993; α_{1S}: Perez-Reyes et al., 1990; Barry et al., 1995). The location of a splice junction identified in the IVS3–S4 region of the α_{1E} gene is indicated (*arrow,* see below). *B*, A comparison of the rat Ca channel α_{1A}, α_{1B}, and α_{1E} genes in the region of the IVS3–S4 linker splice junction. Relevant exon (*upper case*) and intron (*lower case*) sequences are shown together with the splice junction consensus sequences ag-gt (*underlined*). The six base exon encoding ET resides ~8 kb into the 5′ intron of the IVS3–S4 region of the α_{1B} gene (*upper case, shaded*). The putative exon encoding NP in the α_{1A} gene is displayed (*), but its precise location not yet determined. The absence of an intervening exon in the α_{1E} intron is denoted by a *continuous dotted line.* GenBank accession numbers AF146632, AF146633, AF146634.

a pharmacologically and functionally distinct class of Ca channel (Soong et al., 1993). The α_{1E} gene contains a ~700 bp intron in the IVS3–S4 linker region and no obvious intervening exon (Fig. 6*A*). The absence of an alternatively spliced cassette exon in the IVS3–S4 linker region of the α_{1E} gene is consistent with RNase protection analysis of α_{1E} mRNA from rat brain, which revealed no evidence of sequence variations in this IVS3–S4 linker (data not shown). The high degree of sequence homology between α_{1B} and α_{1A} in the IVS3–S4 linker region (Fig. 6*B*) together with the finding that a six-base sequence is alternatively spliced at both of these sites (Fig. 6*A*) suggested that ET and NP share a common functional role. To test this hypothesis we studied the functional impact on N-type Ca channel currents of replacing ET in rn$\alpha_{1B\text{-}b}$ with NP. Figure 5 shows that the +NPα_{1B} mutant gives rise to N-type Ca channel currents in oocytes with gating kinetics indistinguishable from wild type (i.e., +ETα_{1B}).

+NPα_{1A} and ΔNPα_{1A} mRNAs are expressed in different regions of the rat nervous system

Although the presence of variants of the Ca channel α_{1A} that differ in the expression of the NP site has been reported (Yu et al., 1992; Ligon et al., 1998; Sutton et al., 1998; Hans et al., 1999), the distribution of +NPα_{1A} and ΔNPα_{1A} mRNAs in different regions of the rat nervous system have not been quantified. We therefore used the RNase protection analysis to determine the expression pattern of the IVS3–S4 splice variants of α_{1A} (Fig. 7). Low levels of +NP α_{1A} mRNA were found in rat, spinal cord, striatum, and thalamus, a pattern that parallels the low levels of +ET α_{1B} mRNA in the CNS (Fig. 4). However, the pattern of NP expression in the cerebellum, cortex, and hippocampus did not conform to this picture because mRNA isolated from these tissues contained a significant proportion of +NPα_{1A} mRNAs. In fact, in the hippocampus +NPα_{1A} mRNAs dominated (~60%). Consistent with the abundance of +ETα_{1B} mRNAs in peripheral tissue, the majority of α_{1A}mRNA in superior cervical and dorsal root ganglia contained the six bases encoding NP in domain IVS3–S4 of α_{1A}. The absolute level of α_{1A} mRNA expressed in sympathetic neurons was very low as expected from the absence of P-type currents in recordings from rat sympathetic neurons (Mintz et al., 1992).

The differences in the properties of rn$\alpha_{1B\text{-}b}$ (ΔSFMG/+ET) and rn$\alpha_{1B\text{-}d}$ (+SFMG/ΔET) currents may influence action potential-induced Ca entry

We have demonstrated functional differences between splice variants of the N-type Ca channel α_{1B} subunit and shown that they are differentially expressed in peripheral and central neurons. We do not as yet know whether these functional differences are sufficient to influence action potential-dependent Ca entry in neurons. As a first step toward addressing this question we have used standard modeling techniques to predict whether rn$\alpha_{1B\text{-}b}$ (ΔSFMG,+ET) and rn$\alpha_{1B\text{-}d}$ (+SFMG, ΔET) N-type cur-

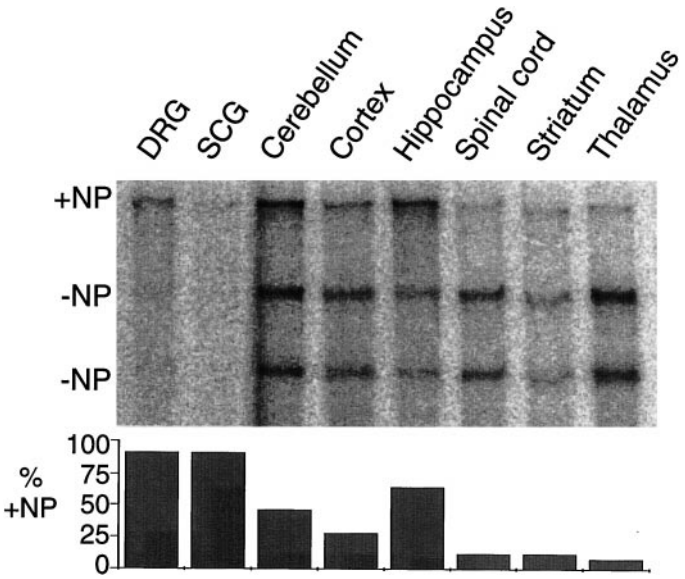

Figure 7. The expression pattern of NPα_{1A} splice variants in various regions of the rat nervous system. RNase protection analysis of α_{1A} RNA isolated from dorsal root ganglia (*DRG*), superior cervical ganglia (*SCG*), and various regions of the brain of adult rats using a probe complimentary to the region of α_{1A} from nt 4605 to nt 4930 and containing the NP insertion at nt 4805. *Top*, Gel separation of RNase-digested ^{32}P-labeled probe hybridized to the various RNA samples. The predominance of fully protected probe (331 nt) in DRG indicates an abundance of +NPα_{1A} RNA, and the presence of two shorter bands (−NP, 200 nt and 125 nt, corresponding to cleaved probe) most prominent in the spinal cord, striatum, and thalamus preps after digestion, indicates that most of α_{1A} RNA in these tissues lacks the NP site. The histogram shows the average levels of +NP containing α_{1A} RNA in at least three experiments. In ganglionic tissue ~80% of the α_{1A} RNA pool contained the NP site. The weak signal in SCG reflects low expression levels of the α_{1A} gene in this tissue. Cerebellum, cortex, and hippocampal RNA contained a mix of +NPα_{1A} and ΔNPα_{1A} RNAs, and in spinal cord, striatum, and thalamic tissue ΔNPα_{1A} RNAs dominated. RNA products were separated on a 5% acrylamide gel, and relative band intensities were calculated using a phosphorimager.

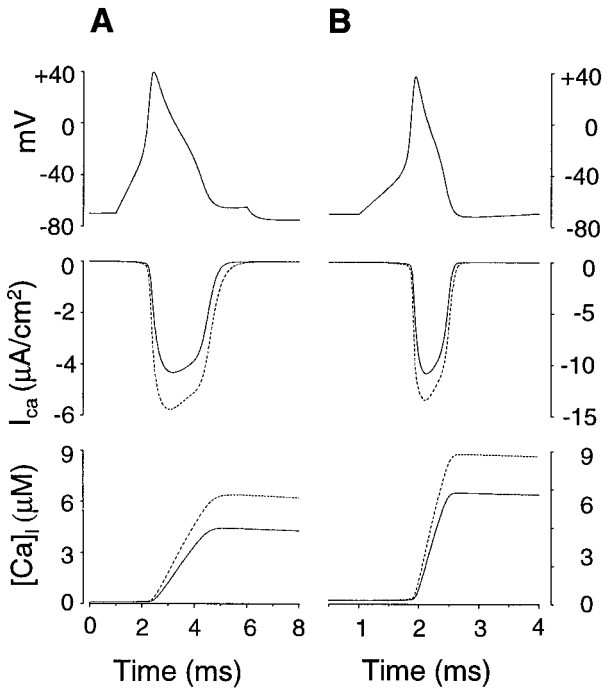

Figure 8. Predicting the impact of alternative splicing in the S3–S4 linkers of the α_{1B} subunit on action potential-dependent Ca influx in a model neuron. A one-compartment model was used to predict the time course and magnitude of calcium entry in a neuron during action potential-induced depolarization at 22°C (*A*) and 37°C (*B*). A simulated action potential evoked by a 5 msec, 400 pA current step (*top*) together with a comparison of the resultant N-type channel current (*middle*) and time course of intracellular calcium concentration (*bottom*) expected in a model neuron expressing either rn$\alpha_{1B\text{-}b}$ (Δ/+, *solid line*) or rn$\alpha_{1B\text{-}d}$ (+/Δ, *dashed line*)-type channels. A shift in the voltage-dependence of the N-type Ca channel conductance activation variable ($m_{\infty,\,Ca}$) by −7 mV and a 1.5-fold decrease in the activation time constant expected for rn$\alpha_{1B\text{-}d}$ compared with rn$\alpha_{1B\text{-}b}$ [Lin et al. (1997a); and see our Fig. 2*A*] results in both an increase in total charge transfer and peak intracellular Ca concentration, respectively, of 46 and 44% at 22°C (*A*) and of 36 and 35% at 37°C (*B*). An accompanying increase in the rate of increase of the intracellular Ca concentration of 1.3-fold at 22° and 37°C was also observed. Channel gating parameters were obtained from measurements at room temperature and were modified for the 37°C simulation based on a Q_{10} of 2.3 for Na and K channels and a Q_{10} of 3.0 for the Ca channel (Cota et al., 1983). We assume that the relative differences in the gating properties of the α_{1B} splice variants observed at room temperature are maintained at 37°C.

rents can, under certain conditions, differentially affect action potential-induced Ca influx in a model neuron. A more direct comparison of the effectiveness of the two Ca channel splice variants for supporting action potential-induced Ca entry in *Xenopus* oocytes is not feasible using conventional two-microelectrode voltage-clamp methods because of the limited temporal resolution associated with cells of this size. Simulated action potentials similar to those recorded in native sympathetic neurons (Yamada et al., 1989) (Fig. 8) were therefore used to trigger voltage-dependent Ca influx in model neurons (Na, K, and Ca current densities of 300, 300, and 1.0 pS/μm^2, respectively) expressing either rn$\alpha_{1B\text{-}b}$ or rn$\alpha_{1B\text{-}d}$ N-type Ca channel currents. Ca channel current densities and peak intracellular Ca concentrations were modeled at room temperature (22°C) (Fig. 8*A*) and at 37°C (Fig. 8*B*). Under these conditions increases in both the total charge transfer and peak intracellular Ca concentration of 45% (at 22°C) and 35% (at 37°C) were observed after an action potential in a neuron expressing rn$\alpha_{1B\text{-}d}$-type Ca channels (Fig. 8, *dashed line*) relative to rn$\alpha_{1B\text{-}b}$ (Fig. 8, *solid line*). The model also predicts a slightly faster rate of rise of the intracellular calcium signal (~1.3-fold) in a neuron expressing rn$\alpha_{1B\text{-}d}$-type Ca channels compared with rn$\alpha_{1B\text{-}b}$.

DISCUSSION

The mammalian genes encoding voltage-gated Ca channel α_1 subunits are large and complex, containing approximately 50 exons, several of which are alternatively spliced (Soldatov, 1994; Yamada et al., 1995; Hogan et al., 1996; Ophoff et al., 1996). With few exceptions (Lin et al., 1997a,b; Sutton et al., 1998; Hans et al., 1999), studies that address the functional consequences of these splicing events have been limited to non-neuronal-derived L-type Ca channel subunits (Klockner et al., 1997; Soldatov et al., 1997; Welling et al., 1997; Zuhlke et al., 1998). Building on our previous studies (Lin et al., 1997a), we now focus on the importance of regulated alternative splicing in the IVS3–S4 linkers of the α_{1B} and closely related α_{1A} subunits.

Two amino acids in the IVS3–S4 extracellular linker of α_{1B} slow N-type Ca channel activation

The S3–S4 linkers of a number of voltage-gated and structurally related ion channels are important in determining the time course

and voltage dependence of channel activation (Perez-Reyes et al., 1990; Nakai et al., 1994; Lin et al., 1997a; Mathur et al., 1997; Tang and Papazian, 1997; Hans et al., 1999). We now demonstrate that alternative splicing of just two amino acids, ET, in domain IVS3–S4 of the Ca channel α_{1B} subunit underlies the different gating kinetics of two previously identified variants, rn$\alpha_{1B\text{-}b}$ and rn$\alpha_{1B\text{-}d}$ (Lin et al., 1997a). We also demonstrate that a chemically dissimilar but functionally homologous dipeptide sequence NP (see below) can fully replace and substitute for ET in domain IVS3–S4 of α_{1B}, showing that the side chains of ET are not unique in contributing to the relatively slow activation kinetics of +ETα_{1B}. The importance of the IVS3–S4 linker in influencing activation of the Ca channel is supported by the high level of conservation of alternative splicing in this region of other α_1 subunits (Fig. 6) (Snutch et al., 1991; Barry et al., 1995; Ihara et al., 1995; Lin et al., 1997a; Ligon et al., 1998; Sutton et al., 1998; Hans et al., 1999). Moreover, in a recent study Hans et al. (1999) compared the functional properties of two variants of the Ca channel α_{1A} subunit that also differed by two amino acids (NP) in the IVS3–S4 linker and showed that the ΔNP variant of α_{1A} activated at a rate 1.7-fold faster compared with +NPα_{1A}. Remarkably, this difference corresponds precisely to that observed between ΔET α_{1B} and +ET α_{1B} (1.5-fold) (Fig. 2). The similar functional consequences of splicing at the ET and NP loci, combined with the high degree of conservation between the IVS3–S4 splice junctions of the α_{1B} and α_{1A} genes, imply a common functional role. α_{1A} and α_{1B} subunits are both critically important for coupling excitation to transmitter release at the majority of synapses throughout the nervous system (Dunlap et al., 1995); thus one consequence of tissue-specific expression of functionally distinct IVS3-S4 splice variants of these proteins might be to optimize the release of neurotransmitters in different regions. +ETα_{1B} and +NPα_{1A} mRNAs that encode relatively slow activating channels (α_{1B}; Fig. 2) (α_{1A}; Hans et al., 1999) dominate in peripheral neurons (Figs. 4, 7), implying that excitation–secretion coupling might be less efficient at postganglionic synapses in comparison with many synapses in the CNS. +NPα_{1A} mRNAs, however, are not solely restricted to peripheral neurons (Fig. 7), implying that different regions within the CNS may contain functionally distinct α_{1A}-containing Ca channels. On the basis of their different ω-aga-IVA sensitivities, Sutton et al. (1988) have proposed that the expression of ΔNPα_{1A} and +NPα_{1A} splice variants correlates with the presence of high (P-type) and low (Q-type) affinity ω-aga-IVA-sensitive Ca channels (Sather et al., 1993; Stea et al., 1994; Wheeler et al., 1994; Randall and Tsien, 1995). Additional studies are needed to test this hypothesis, but our ribonuclease protection analysis (Fig. 7) suggests a reasonable, although not perfect, correlation between the presence of ΔNPα_{1A} mRNA and P-type channels on the one hand and +NPα_{1A} mRNA and Q-type on the other. For example, in DRG neurons the majority of the α_{1A} mRNA pool contains the NP exon (Fig. 7), and in these neurons ω-aga-IVA inhibits the Ca current with relatively slow kinetics (Mintz et al., 1992), not inconsistent with the presence of a Q-type current. In spinal cord, ΔNPα_{1A} mRNA dominates (Fig. 7), and block by ω-aga-IVA is relatively rapid (Mintz et al., 1992) and thus not inconsistent with P-type currents. Furthermore, in the cerebellum and hippocampus, where significant levels of both ΔNPα_{1A} and +NPα_{1A} mRNAs are found (Fig. 7), both P- and Q-type Ca channel currents have been described (Llinas et al., 1989; Wheeler et al., 1994; Randall and Tsien, 1995). The dominance of ΔNP α_{1A} mRNA in the thalamus (Fig. 7), on the other hand, does not correlate well with the significant Q-type current component reported in this region of the brain (Kammermeier and Jones, 1997).

As yet we have no evidence that splice variants of the N-type Ca channel α_{1B} subunit differ in their pharmacological properties. ω-conotoxin GVIA, the widely used high-affinity N-type Ca channel blocker, inhibits both variants equally well (Z. Lin and D. Lipscombe, unpublished observations), consistent with studies of native N-type Ca channels in peripheral and central neurons (Wang et al., 1998). This result is not surprising, however, considering that the IVS3–S4 extracellular linker is not the main site of ω-conotoxin GVIA binding (Ellinor et al., 1994). Drugs or toxins that bind to the S3–S4 linkers of the Ca channel α_{1B} subunit that discriminate between S3–S4 splice variants may be identified in the future. The S3–S4 linkers of several voltage-gated channel α_1 subunits, including α_{1A}, are known to be important targets of toxin binding (Rogers et al., 1996; Swartz and MacKinnon, 1997; Cestele et al., 1998; Sutton et al., 1998; Hans et al., 1999). In the case of the voltage-gated Na channel α subunit, a single amino acid (Gly) within the IIS3–S4 linker plays a major role in β-scorpion toxin binding (Cestele et al., 1998).

Predicting the differential effect of the different Ca channel α_{1B} splice variants on action potential-induced calcium entry

Our modeling provides a useful first step toward understanding how differences in the gating kinetics and voltage dependence of activation between the α_{1B} splice variants might affect action potential-induced Ca entry. Under the specific condition of the model used here, the CNS-dominant Ca channel variant ΔETα_{1B} supports a larger and slightly faster rising intracellular calcium signal in response to action potential-induced depolarization compared with +ETα_{1B} (Fig. 8). However, the significance of these differences with respect to excitation–secretion coupling efficiency at synapses that use the N-type Ca channel is difficult to predict. Neurosecretion is thought to be triggered by intracellular calcium levels in the range of 500 nM to a few micromoles (Augustine and Neher, 1992; Heidelberger et al., 1994), and differences in the rate of rise of the calcium transient may be more important than differences in the absolute levels of calcium. Our model, however, does not take into account how the presence of Ca buffers might shape the Ca signal close to the Ca channel in the microdomain where excitation–secretion coupling occurs (Naraghi and Neher, 1997). Furthermore, many other factors such as (but not limited to) Ca channel density, the shape of the presynaptic action potential, and neurotransmitter and second messenger-mediated Ca and K channel modulation will affect presynaptic calcium levels. For example, the effectiveness of rn$\alpha_{1B\text{-}d}$-type currents to couple depolarization to Ca entry in a neuron is enhanced relative to rn$\alpha_{1B\text{-}b}$ with relatively brief depolarizations, but declines as the stimulus duration is increased. Furthermore, if the N-type Ca channel current activates fully during the rising phase of the action potential, then differences in the rate or voltage dependence of Ca channel opening will have relatively insignificant effects on Ca entry. In contrast, a slowing of Ca channel gating kinetics, such as is observed during G-protein-mediated modulation, would serve to amplify the different effectiveness of the two splice variants to couple depolarization to Ca entry. The primary purpose of the model presented here is to emphasize that although they are small, the functional differences between the α_{1B} splice variants may, under certain conditions, significantly impact action potential-induced Ca entry.

Regulated alternative splicing is an important mechanism used throughout the nervous system for generating functionally distinct products from a single gene in different regions of the nervous system and at different stages during development (Grabowski, 1998). The continued characterization of alternatively spliced loci of Ca channel α_1 subunits in neurons will likely lead to a greater understanding of the scope of Ca channel diversity and the physiological importance of the expression of splice variants in the mammalian nervous system.

REFERENCES

Augustine GJ, Neher E (1992) Calcium requirements for secretion in bovine chromaffin cells. J Physiol (Lond) 450:247–271.

Barry EL, Gesek FA, Froehner SC, Friedman PA (1995) Multiple calcium channel transcripts in rat osteosarcoma cells: selective activation of alpha 1D isoform by parathyroid hormone. Proc Natl Acad Sci USA 92:10914–10918.

Cestele S, Qu Y, Rogers JC, Rochat H, Scheuer T, Catterall WA (1998) Voltage sensor-trapping: enhanced activation of sodium channels by beta-scorpion toxin bound to the S3–S4 loop in domain II. Neuron 21:919–931.

Chomczynski P, Sacchi N (1987) Single-step method of RNA isolation by acid guanidinium thiocyanate-phenol-chloroform extraction. Anal Biochem 162:156–159.

Coppola T, Waldmann R, Borsotto M, Heurteaux C, Romey G, Mattei M-G, Lazdunski M (1994) Molecular cloning of a murine N-type calcium channel α1 subunit. Evidence for isoforms, brain distribution, and chromosomal localization. FEBS Lett 338:1–5.

Cota G, Nicola Siri L, Stefani EJ (1983) Calcium-channel gating in frog skeletal muscle membrane: effect of temperature. J Physiol (Lond) 338:395–412.

Dubel SJ, Starr TV, Hell JW, Ahlijanian MK, Enyeart JJ, Catterall WA, Snutch TP (1992) Molecular cloning of the α_1 subunit of an ω-conotoxin-sensitive calcium channel. Proc Natl Acad Sci USA 89:5058–5062.

Dunlap K, Luebke JI, Turner TJ (1995) Exocytotic Ca^{2+} channels in mammalian central neurons. Trends Neurosci 18:89–98.

Ellinor PT, Zhang J-F, Horne WA, Tsien RW (1994) Structural determinants of the blockade of N-type calcium channels by a peptide neurotoxin. Nature 372:272–275.

Fujita Y, Mynlieff M, Dirksen RT, Kim M-S, Niidome T, Nakai J, Friedrich T, Iwabe N, Miyata T, Furuichi T, Furuichi T, Furutama D, Mikoshiba K, Mori Y, Beam KG (1993) Primary structure and functional expression of the ω-conotoxin-sensitive N-type channel from rabbit brain. Neuron 10:585–598.

Goldin AL, Sumikawa K (1992) Preparation of RNA for injection into *Xenopus* oocytes. Methods Enzymol 207:279–297.

Grabowski PJ (1998) Splicing regulation in neurons: tinkering with cell-specific control. Cell 92:709–712.

Hans M, Urrutia A, Deal C, Brust PF, Stauderman K, Ellis SB, Harpold MM, Johnson EC, Williams ME (1999) Structural elements in domain IV that influences biophysical and pharmacological properties of human α_{1A}-containing high-voltage activated calcium channels. Biophys J 76:1384–1400.

Heidelberger R, Heinemann C, Neher E, Matthews G (1994) Calcium dependence of the rate of exocytosis in a synaptic terminal. Nature 371:513–515.

Hille B (1992) Ionic channels of excitable membranes. Sunderland, MA: Sinauer.

Hines ML, Carnevale NT (1997) The NEURON simulation environment. Neural Comput 9:1179–1209.

Hirning LD, Fox AP, McCleskey EW, Miller RJ, Olivera BM, Thayer SA, Tsien RW (1988) Dominant role of N-type Ca^{2+} channels in evoked release of norepinephrine from sympathetic neurons. Science 239:57–61.

Hogan K, Gregg RG, Powers PA (1996) The structure of the gene encoding the human skeletal muscle alpha 1 subunit of the dihydropyridine-sensitive L-type calcium channel (CACNL1A3). Genomics 31:392–394.

Ihara Y, Yamada Y, Fujii Y, Gonoi T, Yano H, Yasuda K, Inagaki N, Seino Y, Seino S (1995) Molecular diversity and functional characterization of voltage-dependent calcium channels (CACN4) expressed in pancreatic beta-cells. Mol Endocrinol 9:121–130.

Jones SW, Marks TN (1989) Calcium currents in bullfrog sympathetic neurons. II. Inactivation. J Gen Physiol 94:169–182.

Kammermeier PJ, Jones SW (1997) High-voltage-activated calcium currents in neurons acutely isolated from the ventrobasal nucleus of the rat thalamus. J Neurophysiol 77:465–475.

Klockner U, Mikala G, Eisfeld J, Iles DE, Strobeck M, Mershon JL, Schwartz A, Varadi G (1997) Properties of three COOH-terminal splice variants of a human cardiac L-type Ca2+-channel alpha1-subunit. Am J Physiol 272:H1372–1381.

Ligon B, Boyd 3rd AE, Dunlap K (1998) Class A calcium channel variants in pancreatic islets and their role in insulin secretion. J Biol Chem 273:13905–13911.

Lin Z, Haus S, Edgerton J, Lipscombe D (1997a) Identification of functionally distinct isoforms of the N-type Ca^{2+} channel in rat sympathetic ganglia and brain. Neuron 18:153–166.

Lin Z, Lin Y, Lipscombe D (1997b) Alternative splicing in the fourth domain of the Ca channel α_{1B}-subunit can account for the expression of kinetically distinct variants of the N-type Ca channel in the nervous system of the rat. J Physiol (Lond) 504:156.

Llinas R, Sugimori M, Lin JW, Cherksey B (1989) Blocking and isolation of a calcium channel from neurons in mammals and cephalopods utilizing a toxin fraction (FTX) from funnel-web spider poison. Proc Natl Acad Sci USA 86:1689–1693.

Mainen ZF, Sejnowski TJ (1995) Reliability of spike timing in neocortical neurons. Science 268:1503–1506.

Mathur R, Zheng J, Yan Y, Sigworth FJ (1997) Role of the S3–S4 linker in Shaker potassium channel activation. J Gen Physiol 109:191–199.

Miljanich GP, Ramachandran J (1995) Antagonists of neuronal calcium channels: structure, function, and therapeutic implications. Annu Rev Pharmacol Toxicol 35:707–734.

Mintz IM, Adams ME, Bean BP (1992) P-type calcium channels in rat central and peripheral neurons. Neuron 9:85–95.

Nakai J, Adams BA, Imoto K, Beam KG (1994) Critical roles of the S3 segment and S3–S4 linker of repeat I in activation of L-type calcium channels. Proc Natl Acad Sci USA 91:1014–1018.

Naraghi M, Neher E (1997) Linearized buffered Ca^{2+} diffusion in microdomains and its implications for calculation of $[Ca^{2+}]$ at the mouth of a calcium channel. J Neurosci 17:6961–6973.

Olivera BM, Miljanich GP, Ramachandran J, Adams ME (1994) Calcium channel diversity and neurotransmitter release: the omega-conotoxins and omega-agatoxins. Annu Rev Biochem 63:823–867.

Ophoff RA, Terwindt GM, Vergouwe MN, van Eijk R, Oefner PJ, Hoffman SM, Lamerdin JE, Mohrenweiser HW, Bulman DE, Ferrari M, Haan J, Lindhout D, van Ommen GJ, Hofker MH, Ferrari MD, Frants RR (1996) Familial hemiplegic migraine and episodic ataxia type-2 are caused by mutations in the Ca2+ channel gene CACNL1A4. Cell 87:543–552.

Perez-Reyes E, Weil XY, Castellano A, Birnbaumer L (1990) Molecular diversity of L-type calcium channels. Evidence for alternative splicing of the transcripts of three non-allelic genes. J Biol Chem 265:20430–20436.

Randall A, Tsien RW (1995) Pharmacological dissection of multiple types of Ca^{2+} channel currents in rat cerebellar granule neurons. J Neurosci 15:2995–3012.

Rogers JC, Qu Y, Tanada TN, Scheuer T, Catterall WA (1996) Molecular determinants of high affinity binding of alpha-scorpion toxin and sea anemone toxin in the S3–S4 extracellular loop in domain IV of the Na+ channel alpha subunit. J Biol Chem 271:15950–15962.

Sather WA, Tanabe T, Zhang JF, Mori Y, Adams ME, Tsien RW (1993) Distinctive biophysical and pharmacological properties of class A (BI) calcium channel alpha 1 subunits. Neuron 11:291–303.

Schorge S, Lin Y, Lin Z, Lipscombe D (1998) Alternative splicing in the IVS3–S4 linker of neuronal Ca channel α_{1A} and α_{1B} subunits. Soc Neurosci Abstr 24:1327.

Sheng ZH, Rettig J, Takahashi M, Catterall WA (1994) Identification of a syntaxin-binding site on N-type calcium channels. Neuron 13:1303–1313.

Snutch TP, Tomlinson WJ, Leonard JP, Gilbert MM (1991) Distinct calcium channels are generated by alternative splicing and are differentially expressed in the mammalian CNS. Neuron 7:45–57.

Soldatov NM (1994) Genomic structure of human L-type Ca2+ channel. Genomics 22:77–87.

Soldatov NM, Zuhlke RD, Bouron A, Reuter H (1997) Molecular structures involved in L-type calcium channel inactivation. Role of the carboxyl-terminal region encoded by exons 40–42 in alpha1C subunit in

the kinetics and Ca2+ dependence of inactivation. J Biol Chem 272:3560–3566.

Soong TW, Stea A, Hodson CD, Dubel SJ, Vincent SR, Snutch TP (1993) Structure and functional expression of a member of the low voltage-activated calcium channel family. Science 260:1133–1136.

Starr TV, Prystay W, Snutch TP (1991) Primary structure of a calcium channel that is highly expressed in the rat cerebellum. Proc Natl Acad Sci USA 88:5621–5625.

Stea A, Tomlinson WJ, Soong TW, Bourinet E, Dubel SJ, Vincent SR, Snutch TP (1994) Localization and functional properties of a rat brain alpha 1A calcium channel reflect similarities to neuronal Q- and P-type channels. Proc Natl Acad Sci USA 91:10576–10580.

Sutton KG, Zamponi GW, Bourinet E, Soong TW, Snutch TP (1998) Alternative splicing of the α_{1A} gene generates distinct P- or Q-type sensitivity to ω-agatoxin IVA. Soc Neurosci Abstr 24:21.

Swartz KJ, MacKinnon R (1997) Mapping the receptor site for hanatoxin, a gating modifier of voltage-dependent K+ channels. Neuron 18:675–682.

Takahashi T, Momiyama A (1993) Different types of calcium channels mediate central synaptic transmission. Nature 366:156–158.

Tang CY, Papazian DM (1997) Transfer of voltage independence from a rat olfactory channel to the *Drosophila* ether-a-go-go K+ channel. J Gen Physiol 109:301–311.

Tareilus E, Roux M, Qin N, Olcese R, Zhou J, Stefani E, Birnbaumer L (1997) A *Xenopus* oocyte beta subunit: evidence for a role in the assembly/expression of voltage-gated calcium channels that is separate from its role as a regulatory subunit. Proc Natl Acad Sci USA 94:1703–1708.

Turner TJ, Adams ME, Dunlap K (1992) Calcium channels coupled to glutamate release identified by omega-Aga-IVA. Science 258:310–313.

Wang YX, Bezprozvannaya S, Bowersox SS, Nadasdi L, Miljanich G, Mezo G, Silva D, Tarczy-Hornoch K, Luther RR (1998) Peripheral versus central potencies of N-type voltage-sensitive calcium channel blockers. Naunyn Schmiedebergs Arch Pharmacol 357:159–168.

Welling A, Ludwig A, Zimmer S, Klugbauer N, Flockerzi V, Hofmann F (1997) Alternatively spliced IS6 segments of the alpha 1C gene determine the tissue-specific dihydropyridine sensitivity of cardiac and vascular smooth muscle L-type Ca2+ channels. Circ Res 81:526–532.

Wheeler DB, Randall A, Tsien RW (1994) Roles of N-type and Q-type Ca2+ channels in supporting hippocampal synaptic transmission. Science 264:107–111.

Williams ME, Brust PF, Feldman DH, Patthi S, Simerson S, Maroufi A, McCue AF, Velicelebi G, Ellis SB, Harpold MM (1992) Structure and functional expression of an ω-Conotoxin-sensitive human N-type calcium channel. Science 257:389–395.

Yamada WM, Koch C, Adams PR (1989) Multiple channels and calcium dynamics. In: Methods in neuronal modeling (Koch C, Segev I, eds), pp 97–134. Cambridge, MA: MIT.

Yamada Y, Masuda K, Li Q, Ihara Y, Kubota A, Miura T, Nakamura K, Fujii Y, Seino S, Seino Y (1995) The structures of the human calcium channel alpha 1 subunit (CACNL1A2) and beta subunit (CACNLB3) genes. Genomics 27:312–319.

Yu AS, Hebert SC, Brenner BM, Lytton J (1992) Molecular characterization and nephron distribution of a family of transcripts encoding the pore-forming subunit of Ca^{2+} channels in the kidney. Proc Natl Acad Sci USA 89:10494–10498.

Zamponi GW, Snutch TP (1998) Modulation of voltage-dependent calcium channels by G proteins. Curr Opin Neurobiol 8:351–356.

Zamponi GW, Soong TW, Bourinet E, Snutch TP (1996) Beta subunit coexpression and the alpha1 subunit domain I-II linker affect piperidine block of neuronal calcium channels. J Neurosci 16:2430–2443.

Zhang JF, Ellinor PT, Aldrich RW, Tsien RW (1994) Molecular determinants of voltage-dependent inactivation in calcium channels. Nature 372:97–100.

Zuhlke RD, Bouron A, Soldatov NM, Reuter H (1998) Ca2+ channel sensitivity toward the blocker isradipine is affected by alternative splicing of the human alpha1C subunit gene. FEBS Lett 427:220–224.